nature geoscience

Perspective

https://doi.org/10.1038/s41561-023-01305-0

Atmospheric new particle formation from the CERN CLOUD experiment

Received: 10 March 2023

Accepted: 25 September 2023

Published online: 7 November 2023

Check for updates

Jasper Kirkby[1,2] ✉, António Amorim[3], Urs Baltensperger[4], Kenneth S. Carslaw[5], Theodoros Christoudias[6], Joachim Curtius[2], Neil M. Donahue[7], Imad El Haddad[4], Richard C. Flagan[8], Hamish Gordon[7], Armin Hansel[9], Hartwig Harder[10], Heikki Junninen[11], Markku Kulmala[12,13], Andreas Kürten[2], Ari Laaksonen[14], Katrianne Lehtipalo[12,13], Jos Lelieveld[6,10], Ottmar Möhler[15], Ilona Riipinen[16], Frank Stratmann[17], Antonio Tomé[18], Annele Virtanen[19], Rainer Volkamer[20], Paul M. Winkler[21] & Douglas R. Worsnop[12,14,19,22]

Aerosol particles in the atmosphere profoundly influence public health and climate. Ultrafine particles enter the body through the lungs and can translocate to essentially all organs, and they represent a major yet poorly understood health risk. Human activities have considerably increased aerosols and cloudiness since preindustrial times, but they remain persistently uncertain and underrepresented in global climate models. Here we present a synthesis of the current understanding of atmospheric new particle formation derived from laboratory measurements at the CERN CLOUD chamber. Whereas the importance of sulfuric acid has long been recognized, condensable vapours such as highly oxygenated organics and iodine oxoacids also play key roles, together with stabilizers such as ammonia, amines and ions from galactic cosmic rays. We discuss how insights from CLOUD experiments are helping to interpret new particle formation in different atmospheric environments, and to provide a mechanistic foundation for air quality and climate models.

Particle nucleation gives rise to around half of global cloud condensation nuclei (CCN), and the majority of those in the upper troposphere[1]. Nucleation refers to a phase transformation from a vapour to a critical molecular cluster (nucleus of ~1 nm size) where the Gibbs free energy reaches a maximum. As nucleation must overcome this energy barrier, the rate at which stable particles appear is generally much slower than the kinetic collision rate. New particle formation (NPF) rates are reported in the Cosmics Leaving Outdoor Droplets (CLOUD)

[1]CERN, European Organisation for Nuclear Research, Geneva, Switzerland. [2]Institute for Atmospheric and Environmental Sciences, Goethe University Frankfurt am Main, Frankfurt am Main, Germany. [3]CENTRA and Faculdade de Ciências, University of Lisbon, Lisbon, Portugal. [4]Laboratory of Atmospheric Chemistry, Paul Scherrer Institute, Villigen, Switzerland. [5]School of Earth and Environment, University of Leeds, Leeds, UK. [6]Climate and Atmosphere Research Center, The Cyprus Institute, Nicosia, Cyprus. [7]Center for Atmospheric Particle Studies, Carnegie Mellon University, Pittsburgh, PA, USA. [8]Division of Chemistry and Chemical Engineering, California Institute of Technology, Pasadena, CA, USA. [9]Institute of Ion Physics and Applied Physics, University of Innsbruck, Innsbruck, Austria. [10]Atmospheric Chemistry Department, Max Planck Institute for Chemistry, Mainz, Germany. [11]Institute of Physics, University of Tartu, Tartu, Estonia. [12]Institute for Atmospheric and Earth System Research (INAR), Faculty of Science, University of Helsinki, Helsinki, Finland. [13]Helsinki Institute of Physics, University of Helsinki, Helsinki, Finland. [14]Finnish Meteorological Institute, Helsinki, Finland. [15]Institute of Meteorology and Climate Research, Karlsruhe Institute of Technology, Karlsruhe, Germany. [16]Bolin Centre for Climate Research, Stockholm University, Stockholm, Sweden. [17]TROPOS, Leibniz Institute for Tropospheric Research, Leipzig, Germany. [18]Institute Infante Dom Luíz, University of Beira Interior, Covilhã, Portugal. [19]Department of Applied Physics, University of Eastern Finland, Kuopio, Finland. [20]Department of Chemistry & CIRES, University of Colorado at Boulder, Boulder, CO, USA. [21]Faculty of Physics, University of Vienna, Vienna, Austria. [22]Aerodyne Research Inc., Billerica, MA, USA. ✉e-mail: jasper.kirkby@cern.ch

experiment[2] at CERN, the European Council for Nuclear Research, as the measured flux of particles passing a threshold size (1.7 nm), so the formation rate depends also on the growth rate and ambient condensation sink from scavenging by pre-existing particles. The condensation sink (vapour wall loss rate) for CLOUD is 2.2×10^{-3} s^{-1}, which is comparable to the pristine boundary layer[3]. CLOUD precisely controls all experimental parameters at tropospheric conditions and maintains ultra-low contaminants (Extended Data Tables 1 and 2). All processes are measured at the molecular level to confirm that contaminants do not bias the results.

Over the past decade, huge progress has been made towards a fundamental understanding of the mechanisms and vapours driving NPF in the atmosphere, as illustrated in Fig. 1. These advances are the result of synergy between field observations, aerosol and climate models, quantum chemical calculations, and laboratory measurements. There have been several excellent recent comprehensive reviews of atmospheric NPF[4] and of observations at field[5], mountain[6] and urban[7] sites. We cannot do justice here to the extensive foundational research addressed in those reviews; instead, we present a Perspective confined to the findings revealed by laboratory experiments at the CERN CLOUD chamber and how they relate to the actual atmosphere.

Acid–base nucleation

Sulfuric acid–ammonia

When CLOUD experiments started in 2009, laboratory measurements of binary nucleation of sulfuric acid (H_2SO_4) and water disagreed with each other by many orders of magnitude, making it impossible to resolve whether or not H_2SO_4 alone could account for NPF throughout the atmosphere (except for iodic particles in limited coastal regions[8]). The role of ions for NPF in the troposphere was experimentally unknown, although modelling studies had anticipated their importance[9]. The first experiments at CLOUD[2] showed that binary sulfuric acid nucleation is around 10^5 times too slow to account for NPF in the warm boundary layer (Fig. 2). However, the nucleation rates increase more than 100-fold in the presence of ammonia (NH_3) at only 100 parts per trillion by volume (pptv) (Fig. 2). Ions from galactic cosmic rays increase the nucleation rates by up to a factor of 10. This first paper from CLOUD[2] revealed molecules sticking together and growing into particles under atmospheric conditions, measured with the newly developed Atmospheric Pressure Interface Time-of-Flight (APiTOF) mass spectrometer. The nucleating clusters displayed clear stoichiometry, adding one NH_3 molecule for each additional H_2SO_4 molecule[2,10], which has been confirmed using quantum chemical methods[11]. The formation of acid–base pairs (salts) is perhaps the most important fundamental mechanism underpinning particle nucleation in the atmosphere.

Although atmospheric concentrations of ammonia and sulfuric acid are generally insufficient to account for NPF observed in the warm boundary layer (Fig. 2), the nucleation rates increase rapidly at cooler temperatures[12,13]. In the upper troposphere, nucleation of sulfuric acid with <10 pptv ammonia proceeds near the kinetic limit, that is, it is controlled solely by the molecular collision rate and is, therefore, barrierless nucleation. Ternary H_2SO_4–NH_3–H_2O nucleation has now been observed in the free troposphere at Jungfraujoch, Switzerland (3,570 m altitude)[14], and Chacaltaya, Bolivia (5,240 m)[15]. It is also reported in the cool boundary layer in the boreal forest[16], and near the Antarctic[17] and Arctic[18] coasts where NH_3 is available from seabird colonies. Binary H_2SO_4–H_2O nucleation has also been observed near the Antarctic coast[17]. These ambient observations are indicated in Fig. 3.

Sulfuric acid vapour is mainly produced by the oxidation of sulfur dioxide (SO_2). The principal gas-phase reaction is $SO_2 + OH^{\bullet} + M \rightarrow HOSO_2^{\bullet} + M$ followed by $HOSO_2^{\bullet} + O_2 \rightarrow HO_2^{\bullet} + SO_3$, after which sulfur trioxide reacts rapidly with two water molecules to form sulfuric acid. In some locations, SO_2 may also be oxidized by carbonyl oxides (RR′C = OO) known as stabilized Criegee intermediates[19]. Currently, fossil fuels account for about 75% of global sulfur emissions. However, the dominant source of SO_2 in the marine atmosphere is from oxidation of dimethyl sufide, DMS (CH_3SCH_3), which is emitted from phytoplankton at the sea surface. As well as sulfuric acid, oxidation of DMS produces methanesulfonic acid, MSA (CH_3SO_3H), with a high yield that exceeds that of H_2SO_4 below 10 °C (ref. 20). MSA is also likely to nucleate via an acid–base mechanism with ammonia[21], but experiments at atmospheric conditions remain ambiguous because MSA and H_2SO_4 always appear together from DMS oxidation.

Sulfuric acid–amines

Closely related to ammonia are amines, in which one or more of the hydrogen atoms is replaced by an organic group. Experiments at CLOUD showed that the presence of only 4 pptv dimethylamine, DMA ($(CH_3)_2NH$), can enhance ternary sulfuric acid particle formation rates 1-million-fold compared with ammonia[22] (Fig. 2). The importance of amines over ammonia had been anticipated by quantum chemical studies[23]. These experiments were repeated with a newly developed Chemical Ionization APiTOF (CI-APiTOF), which passes the air sample through a nitrate (NO_3^-) soft-ionization section before entering the APiTOF. This provided the first measurements of neutral (uncharged) molecular clusters during nucleation[24]. The composition of the smallest neutral clusters is perturbed by the chemical charging process. Formation of an HSO_4^- anion (a strong Lewis base) displaces one DMA molecule so the first cluster with DMA is the acid trimer[24,25]. However, after taking this into account, the detected clusters faithfully track the chemistry, appearance time and growth of the neutral clusters. H_2SO_4–DMA nucleation is found to follow the same 1:1 acid–base stoichiometry[22,24,26] as for H_2SO_4–NH_3, which is supported by many quantum chemical studies, for example, the Supplementary Information in ref. 22. A subsequent re-analysis of these data and comparison with a kinetic model[27] shows that, below 278 K, both charged and neutral H_2SO_4–DMA nucleation proceed at the kinetic limit for sulfuric acid (Fig. 2).

For particles above 1.8 nm diameter and at all temperatures below 20 °C, CLOUD measurements show that sulfuric acid condenses at the kinetic limit, regardless of the availability of NH_3 or amines[27,28]. At 1×10^7 cm^{-3} H_2SO_4 (0.4 pptv), the particle growth rate is 1.8 nm h^{-1} between 1.8 and 3.2 nm, slowing to 1.1 nm h^{-1} between 3.2 and 8 nm (ref. 28). Owing to attractive van der Waals forces between the permanent (monomer) and induced (particle) dipoles, the particle growth rates measured below 10 nm exceed the hard-sphere kinetic limit by about a factor of 2. During sulfuric acid–amine NPF, a major contribution to particle growth arises from clusters containing several sulfuric acid–DMA pairs, which are 'hidden' from measurements of the sulfuric acid (monomer) concentration[29,30].

Amines are frequently at the few-pptv level in the continental boundary layer[31,32], sufficient to trigger kinetically-limited nucleation of sulfuric acid particles. As urban environments often have high condensation sinks, above 0.01 s^{-1}, smog episodes initiated by NPF require a fast nucleation mechanism and rapid initial particle growth up to around 10 nm, where the scavenging loss rate slows by an order of magnitude. Indeed, H_2SO_4–DMA is reported to be the dominant nucleation mechanism in Shanghai[33] and to contribute in Beijing[25,34]. This confirms earlier observations in Tecámac, Mexico, and Atlanta that aminium salts form a major component of nucleation mode (<10 nm) aerosol at urban sites[32,35] as well as in the remote Sierra Nevada mountains, California[36] (Fig. 3). Sulfuric acid–amine NPF has also been observed over the open ocean and coast around the pristine Antarctic Peninsula, where amines are emitted from the ocean surface and melting sea ice[37].

Oxygenated organic molecules

Biogenic organic vapours

Most organic vapours in the atmosphere are biogenic. The estimated total annual emissions are 760 Tg (C) yr^{-1}, comprising 70% isoprene

https://doi.org/10.1038/s41561-023-01305-0

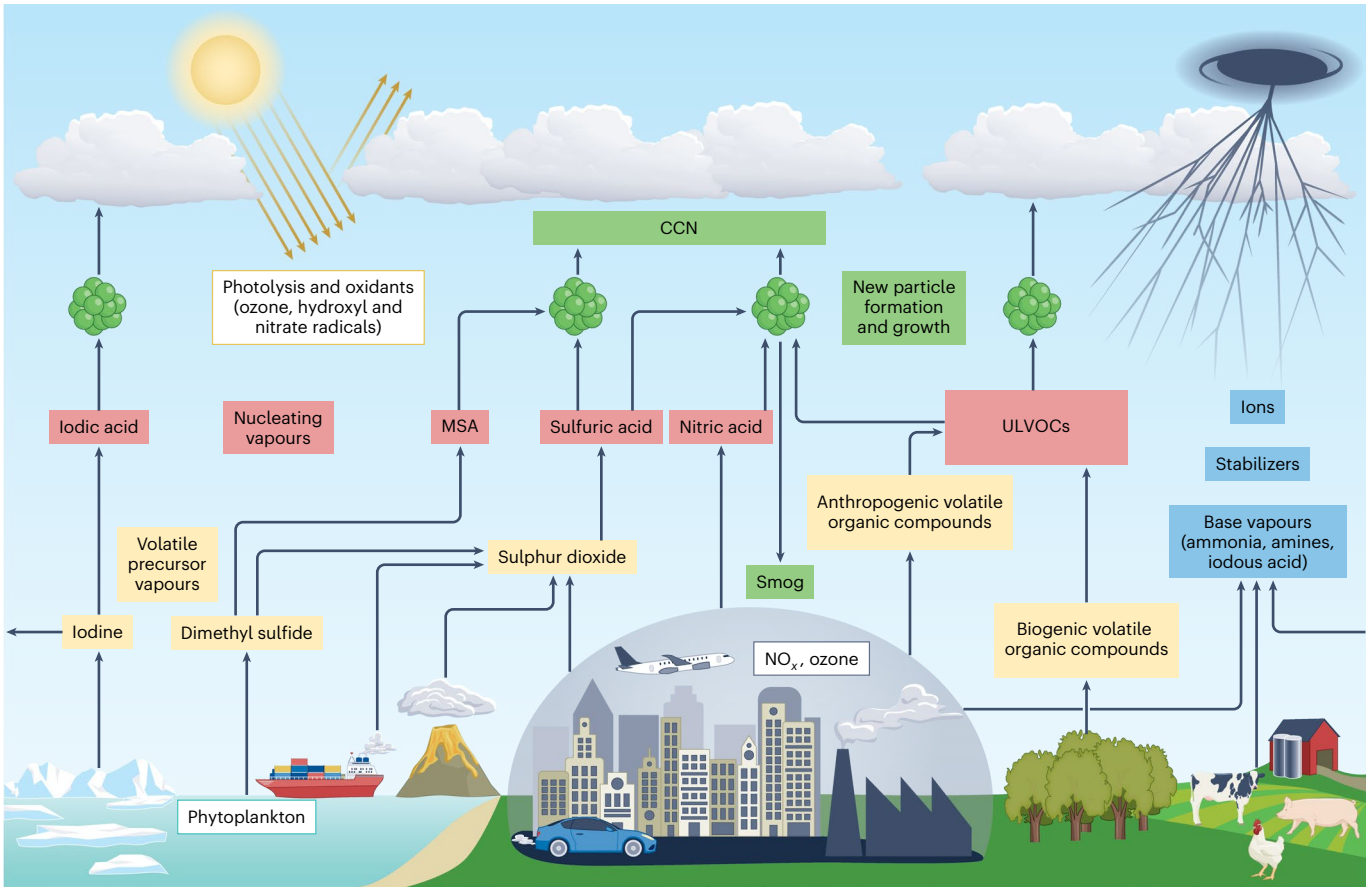

Fig. 1 | Mechanisms for NPF in the atmosphere. Nucleating vapours are indicated in red boxes: sulfuric acid, methanesulfonic acid (MSA, likely), ultra-low-volatility organic compounds (ULVOCs), iodic acid and, under certain conditions, nitric acid. Stabilizers, which reduce evaporation of the embryonic molecular clusters, are indicated in blue boxes: ammonia, amines, iodous acid and ions from galactic cosmic rays (water is also a weak stabilizer but is not indicated as it is ubiquitous in the troposphere). Atmospheric oxidants—especially hydroxyl radicals ($OH^{\bullet}$) and ozone—transform volatile precursor vapours such as sulfur dioxide, dimethyl sulfide, iodine or organic compounds into ultra-low-volatility vapours (for example, ULVOC have saturation vapour concentrations below around 1 molecule cm^{-3}). Ultra-low-volatility vapours may nucleate to form new particles, which can then grow by further vapour condensation to become CCN. NPF and growth occurs essentially throughout the troposphere and, at elevated vapour concentrations, is also responsible for smog episodes in highly polluted urban environments.

(C_5H_8), 11% monoterpenes ($C_{10}H_{16}$, of which about half is α-pinene), 2.5% sesquiterpenes ($C_{15}H_{24}$) and 16% other compounds, mainly ones with fewer carbon atoms[38]. Isoprene is mainly emitted by deciduous trees, whereas conifers are the main source of terpenes. These molecules are characterized by at least one olefinic double bond that renders them highly reactive in the atmosphere. In particular, monoterpenes are rapidly oxidized by ozone or hydroxyl radicals ($OH^{\bullet}$) to form peroxy radicals ($ROO^{\bullet}$), which can, in some circumstances, undergo multiple autoxidation steps to form more highly oxygenated peroxy radicals (Fig. 4). Autoxidation involves successive steps of internal H-atom transfer followed by addition of molecular oxygen. The process is terminated by radical–radical reactions that generate monomers or even covalently bound dimers (ROOR′) with ultra-low volatility[39]. Highly oxygenated organic molecules (HOM) are the subset with six or more oxygen atoms[40]. Experiments at CLOUD discovered that HOM produced by ozonolysis of α-pinene rapidly form particles at atmospheric concentrations and in the absence of sulfuric acid[41]—termed pure organic nucleation (Fig. 2). Ions from galactic cosmic rays (both polarities) increase the nucleation rates by a factor of 10–100 compared with neutral nucleation. The reason for this strong enhancement is that ions reduce the cluster evaporation rates, allowing more organic compounds (with slightly higher volatility) to participate.

Figure 4 illustrates the remarkable ability of the autoxidation mechanism to reduce the volatility of some organic vapours by up to 19 orders of magnitude after only a few minutes exposure to atmospheric oxidants. Ultra-low-volatility organic compounds (saturation mass concentration, $c^0 < 3 \times 10^{-9}$ µg m^{-3}) can nucleate even at extremely low ambient concentrations. Extremely-low-volatility organic compounds ($3 \times 10^{-9} < c^0 < 3 \times 10^{-5}$ µg m^{-3}) can condense on the smallest molecular clusters and drive early growth. Low-volatility organic compounds ($3 \times 10^{-5} < c^0 < 0.3$ µg m^{-3}) can condense on particles above 3–5 nm diameter. Semi-volatile organic compounds ($0.3 < c^0 < 300$ µg m^{-3}) may partition to particles in high-concentration conditions such as photochemical smog. Intermediate-volatility organic compounds ($300 < c^0 < 3 \times 10^6$ µg m^{-3}) and volatile organic compounds ($c^0 > 3 \times 10^6$ µg m^{-3}) remain in the gas phase.

While previous studies have indicated the importance of acid functional groups for organic nucleation[42,43], our perspective from CLOUD experiments is that the principal attribute that determines whether an organic compound will participate in nucleation is its volatility—more specifically, its vapour pressure relative to its equilibrium vapour pressure at the ambient temperature, that is, its saturation ratio. We find that volatility alone—without any consideration of specific functional groups—can explain all our experimental measurements of both nucleation rates and growth rates versus particle size, with either biogenic or anthropogenic organic vapours. Hence the importance of the volatility distribution at the ambient temperature (Fig. 4) rather than functional groups or degree of oxygenation. In the warm boundary layer, the

https://doi.org/10.1038/s41561-023-01305-0

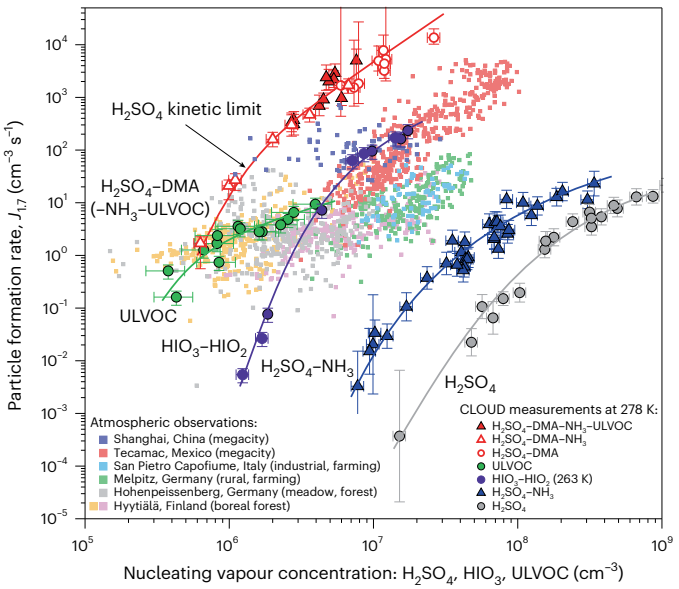

Fig. 2 | Particle formation rates versus vapour concentrations for different chemical systems. The CLOUD particle formation rates are measured at 1.7 nm ($J_{1.7}$) for sulfuric acid (H_2SO_4; grey circles)[22], H_2SO_4 with 2–250 pptv ammonia (NH_3; blue triangles)[22], iodic acid (HIO_3) with around 0.01–0.02 pptv iodous acid (HIO_2; purple circles)[69], pure biogenic ULVOC (green circles)[46], H_2SO_4 with 40 pptv DMA (open red circles)[27], H_2SO_4 with 4 pptv DMA and 1–2 ppbv NH_3 (open red triangles)[67], and H_2SO_4 with 4 pptv DMA, 1–2 ppbv NH_3 and anthropogenic ULVOC from 3–9 ppbv aromatic vapours (filled red triangles)[67]. Water is implicit in all chemical systems. All data are measured under galactic cosmic ray ionization conditions at 278 K except for HIO_3–HIO_2, where neutral (uncharged) and galactic cosmic ray measurements are combined at 263 K. The red curve shows the kinetic limit for sulfuric acid, which coincides with CLOUD measurements of H_2SO_4 with more than 4 pptv DMA, regardless of the presence of additional NH_3 or ULVOC. Other curves are drawn to guide the eye. Observations in the atmospheric boundary layer of NPF rates versus sulfuric acid are indicated by small coloured squares (the references for these atmospheric data are provided in refs. 22,67). The error bars indicate ±1 σ measurement uncertainties. A systematic scale uncertainty on the vapour concentrations of up to a factor of 2 is not shown in the horizontal error bars.

ULVOC dimers are key to pure organic nucleation[41,44]. At lower temperatures, oxygenated monomers also have volatilities in the ULVOC range, and so nucleate[45,46]. Although the rate of autoxidation slows at lower temperatures[39], producing less-oxygenated compounds, their lower volatility almost exactly compensates so that pure biogenic nucleation rates remain high between the warm boundary layer (25 °C) and cold upper troposphere (−50 °C)[45–47]. Following nucleation, our experiments show that the combined ultra-low-volatility, extremely-low-volatility and low-volatility organic compound components can quantitatively account for rapid particle growth rates measured between −25 °C and 25 °C[48,49]. The growth rates are sensitive to particle curvature, showing a 5-fold increase between 1.8 and 5 nm as the Kelvin (curvature) barrier falls away[49], and explaining atmospheric observations of accelerating growth rates over this size range[50]. At colder temperatures, measurements of particle-phase composition confirm enhanced uptake of less-oxygenated compounds due to their reduced volatility[49].

High monoterpene concentrations of up to ~1 part per billion by volume (ppbv) are found in the boreal forest as well as in the Amazon rainforest. However, in contrast with the boreal forest, NPF is rarely observed in the Amazon boundary layer. The reason is likely to be suppression of NPF by isoprene[51,52] in the Amazon rainforest, where concentrations are 3–5 ppbv compared with below 20 pptv in the boreal forest. The presence of isoprene reduces the yield of ULVOC C_{19}–C_{20} dimers, while increasing higher-volatility C_{14}–C_{15} dimers[52]. Indeed, any radicals that reduce the ULVOC yield, such as hydroperoxyl ($HO_2^{\bullet}$) or NO (ref. 53) radicals, reduce biogenic NPF rates. At low concentrations (<100 pptv), however, NO enhances HOM formation[54]. On the other hand, sesquiterpenes promote NPF by increasing the yield of ULVOC C_{20}–C_{30} covalently bound dimers. The NPF rate is doubled by a molar addition of only 2% sesquiterpene to a 10:1 mixture of isoprene to monoterpene[55].

Although largely absent in the Amazon rainforest itself, there is copious NPF overhead in convective cloud outflows at altitudes between 8 and 15 km[56]. Similarly, on a much broader scale, intense NPF has been observed in the tropical upper free troposphere over both the Pacific and Atlantic oceans, covering about 40% of Earth's surface[57]. Biogenic organic vapours are a promising candidate to explain these observations[41,58] (Fig. 3). After long-range transport and air subsidence, this may be a major source of CCN for shallow liquid clouds (stratus and stratocumulus) over oceans[59], which dominate the cloud radiative effect on climate.

The importance of pure biogenic NPF is that it provides a copious source of new particles in pristine environments such as the pre-industrial climate or Earth's future climate without SO_2 emissions. Biogenic NPF raises the baseline preindustrial aerosol state from which anthropogenic aerosol radiative forcing is determined[60], thereby reducing its magnitude[61] and, in turn, estimates of Earth's climate sensitivity. Although there are few truly pristine regions remaining in the present-day atmosphere, biogenic organic NPF has been identified in the boreal forest, Finland[62], at the Pyramid station, Himalayas (5,050 m)[63] and in the sub-boreal forest of North America[64] (Fig. 3). In addition, intense nocturnal NPF has been reported in a eucalyptus forest at Tumbarumba, New South Wales[65]. As sulfuric acid levels are extremely low in the absence of sunlight, nocturnal NPF in forested environments is probably due to pure biogenic organic nucleation.

Anthropogenic organic vapours

Anthropogenic aromatic hydrocarbons are frequently found in cities at total concentrations of a few parts per billion by volume. Experiments at CLOUD have studied NPF from toluene ($CH_3C_6H_5$), trimethylbenzene ($(CH_3)_3C_6H_3$), naphthalene ($C_{10}H_8$) and cresol ($CH_3(C_6H_4)OH$). These vapours are oxidized during daylight hours by hydroxyl radicals (Fig. 4b) to produce high concentrations of oxygenated organic compounds[66] that generate rapid particle growth around 10 nm h^{-1} during smog episodes[67]. While naphthalene can drive pure anthropogenic organic nucleation, the rates are too slow to provide substantial NPF in urban environments, where condensation sinks are high[67].

Particle-phase volatility measurements confirm that the oxidation products of naphthalene or toluene can contribute to the initial growth of newly formed particles[66]. Toluene (C_7) oxidation products have a similar volatility distribution to those from α-pinene (C_{10}), while naphthalene (C_{10}) oxidation products are much less volatile. Rapid progression through multiple generations of $OH^{\bullet}$ reaction is more pronounced in toluene and naphthalene than in α-pinene because the products become progressively more reactive with $OH^{\bullet}$ at each step[66]. Moreover, the reactions favour functional groups with lower volatility per added oxygen atom, such as hydroxyl (OH) and carboxylic (C(=O)OH) groups instead of hydroperoxide (OOH) groups[66]. Consequently, for the same carbon number and fewer oxidation steps, oxygenated aromatic vapours are orders-of-magnitude less volatile than oxygenated biogenic vapours—as seen by comparing Fig. 4a,b. In urban settings, naphthalene is likely to contribute to nucleation and the growth of the smallest particles, whereas the more abundant alkyl benzenes may overtake naphthalene once the Kelvin barrier has fallen away[66,67].

Iodine oxoacids

Seaweeds accumulate iodide as an inorganic antioxidant. Coastal seaweeds release high levels of iodide upon exposure to the atmosphere at low tide, which reacts with ozone in the film of water on the seaweed to

https://doi.org/10.1038/s41561-023-01305-0

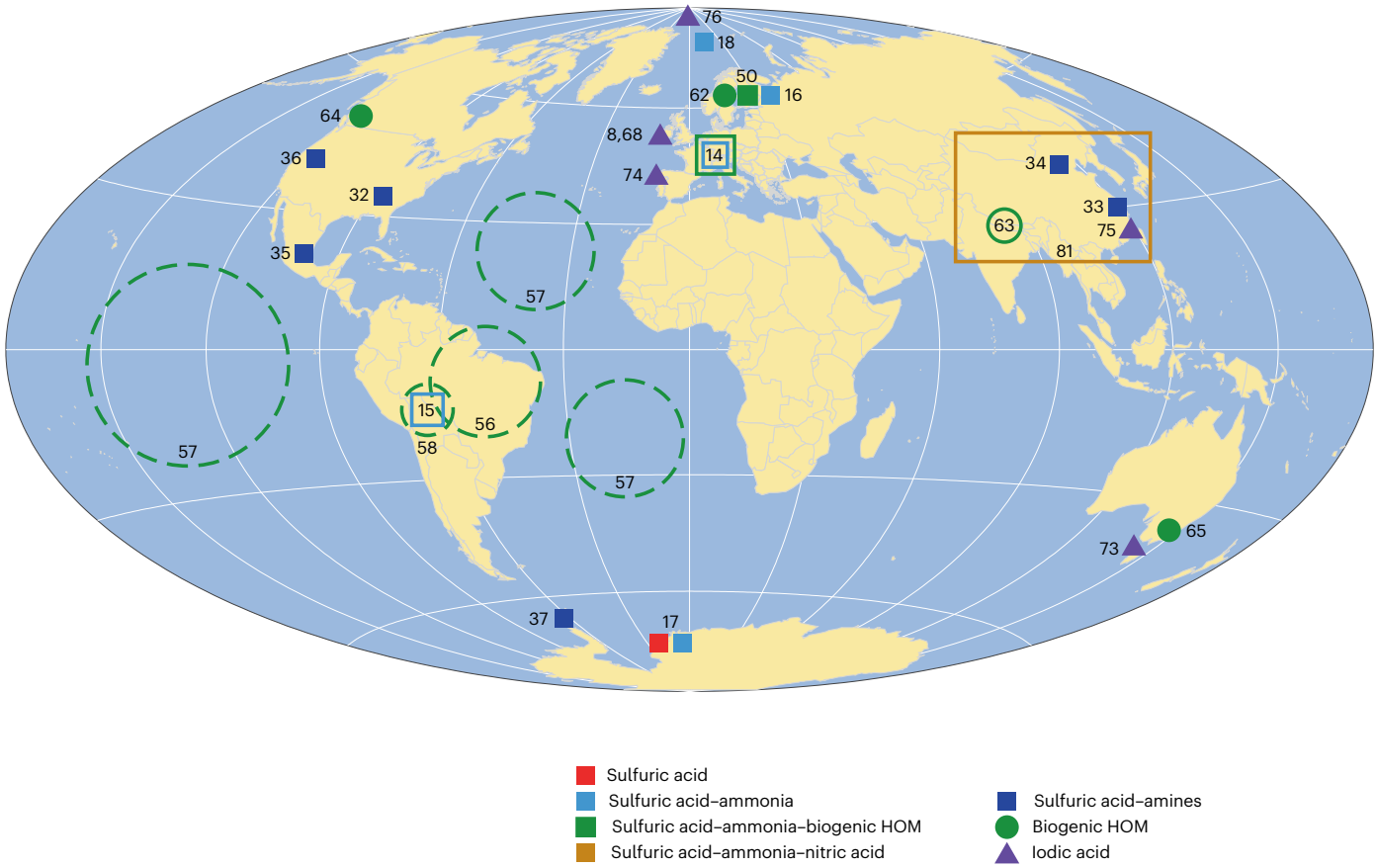

Fig. 3 | Geographical locations of nucleation mechanisms measured in the laboratory by CLOUD. Geographical locations where nucleation mechanisms measured by CLOUD have been identified or inferred from field, mountain and aircraft observations. Filled symbols indicate boundary layer sites and large open symbols indicate the free troposphere; the combined symbol shape plus colour indicate the chemical compounds involved. Dashed symbols indicate likely mechanisms that are as yet unconfirmed by observations. The reference numbers are indicated next to each symbol.

emit molecular iodine. Molecular iodine is then photolysed to iodine radicals ($I^{\bullet}$), which rapidly oxidize to form various compounds, among which are iodine oxoacids: iodic acid (HIO_3) and iodous acid (HIO_2). Observations at Mace Head on the west coast of Ireland have linked iodine emissions with high NPF rates[8]; subsequent measurements at the same site have identified the source as nucleation of iodic acid molecules, which combine in pairs in the particle to form diiodine pentoxide: $HIO_3 + HIO_3 \rightarrow I_2O_5 + H_2O$ (ref. 68).

Laboratory experiments at CLOUD have confirmed this mechanism for charged (ion-induced) nucleation but have shown that uncharged (neutral) nucleation proceeds via repeated stepwise condensation of iodic acid followed by iodous acid[69]. The iodine oxoacids then combine in the particle to form diiodine tetroxide: $HIO_3 + HIO_2 \rightarrow I_2O_4 + H_2O$. Quantum chemical calculations have confirmed the importance of iodous acid, which acts as a base (proton acceptor) to stabilize iodic acid in neutral molecular clusters[70]. The nucleation rates of HIO_3 particles are rapid, greatly exceeding H_2SO_4–NH_3 rates at similar acid concentrations[69] (Fig. 2). Ion-induced nucleation proceeds at the kinetic limit below +10 °C but is limited by the ion-pair production rate in the boundary layer (2–10 cm^{-3} s^{-1}).

The CLOUD experiments used green illumination to photolyse molecular iodine without producing hydroxyl radicals from ozone in the chamber. This revealed a new and highly efficient chemical pathway for producing iodic acid via iodooxy hypoiodite, I_2O_2, which can explain daytime observations of HIO_3 production in the remote lower troposphere[71]. Iodooxy hypoiodite is rapidly produced in weak daylight from $I^{\bullet} + O_3 \rightarrow IO^{\bullet} + O_2$ followed by $IO^{\bullet} + IO^{\bullet} \rightarrow IOIO$, and then iodic acid is produced from the reactions $IOIO + O_3 \rightarrow IOIO_4$ followed by $IOIO_4 + H_2O \rightarrow HIO_3 + HOI + O_2$. The growth of charged or neutral iodine oxoacid particles to CCN sizes is driven almost entirely by the more abundant acid, HIO_3, which condenses at the kinetic limit[69]. Direct measurements of particles above a few nanometres show that they comprise essentially pure HIO_3, indicating that the dehydration mechanism to form iodine oxides is important only for nucleation and not later growth.

Overall, therefore, iodic acid is a highly efficient potential source of NPF in the boundary layer: it competes with H_2SO_4–NH_3 in pristine regions; proceeds in overcast daylight; a single precursor vapour drives both rapid nucleation and growth; and iodine is ubiquitous in the atmosphere[69,71]. Iodine emissions from the sea surface have tripled since 1950[72] and are projected to keep increasing as ozone concentrations rise and sea ice retreats. Moreover, there may be a catalytic role of iodine in NPF because particulate iodate is readily reduced, recycling iodine back into the gas phase. As well as western Ireland (Mace Head)[8,68], iodine-driven nucleation has been identified near the coasts of Tasmania (Cape Grim)[73], northwest Spain (O Grove, Galicia)[74] and China (Xiangshan Gulf)[75] (Fig. 3). Furthermore, although measurements over the remote ocean are sparse, frequent NPF over the high Arctic pack ice has recently been reported, driven by iodic acid with little contribution from sulfuric acid[76].

Mixed chemical systems

Sulfuric acid–amines–ammonia–organic vapours

In regions where DMA is below a few parts per trillion by volume, mixtures of different amine compounds and ammonia are found to nucleate synergistically with sulfuric acid[26,34,77]. Experiments at CLOUD have

https://doi.org/10.1038/s41561-023-01305-0

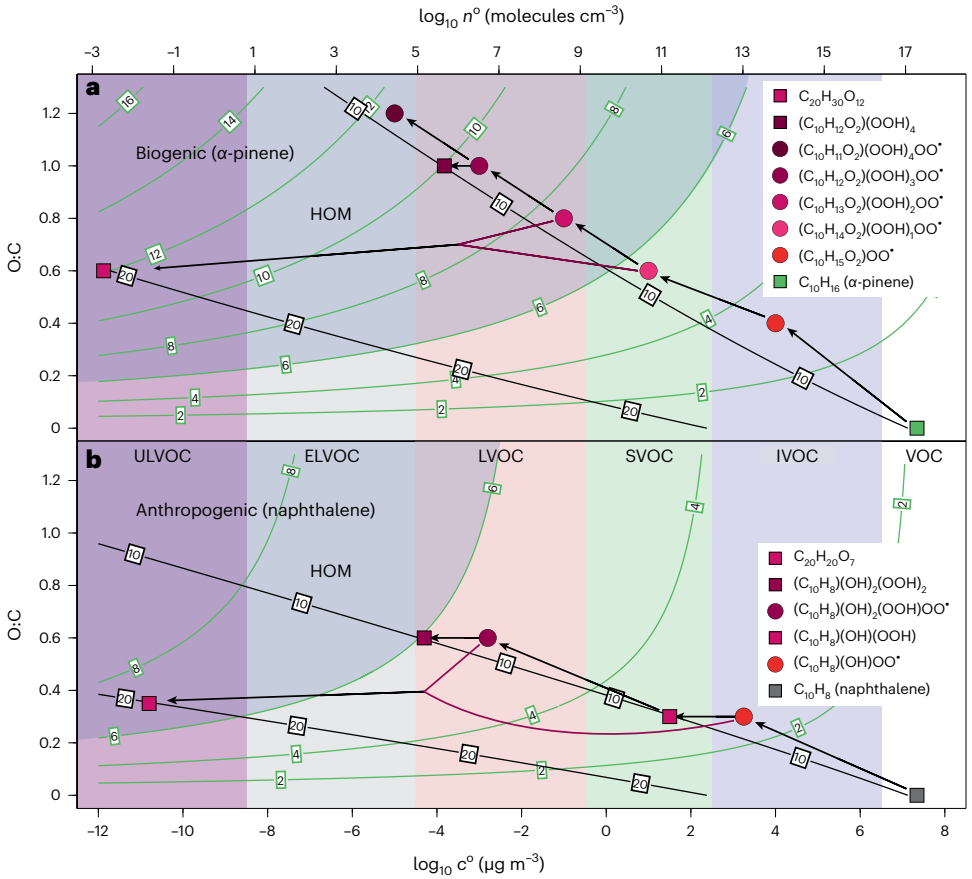

Fig. 4 | Two-dimensional volatility basis set for oxidation of biogenic and anthropogenic organic vapours[100]. Oxygen-to-carbon ratio (O:C) versus $\log_{10}$ saturation concentration, c^0 (lower axis), and corresponding $\log_{10}$ number concentration, n^0 (upper axis), shown for the indicated compounds at 300 K. Carbon number is shown by black contours and oxygen number by green contours. HOM have at least six oxygen atoms and are indicated by darker shading. Increased oxygenation leads to lower volatility and increased importance for NPF (coloured bands; see text for details). **a**, Biogenic organic vapours such as α-pinene (green square) are rapidly oxidized by ozone to produce peroxy radicals (starting with $(C_{10}H_{15}O_2)OO^•$), indicated by red circles. Some of these peroxy radicals undergo autoxidation involving successive steps of internal H-atom transfer followed by molecular oxygen addition. Each step adds a hydroperoxy (OOH) functional group and creates a new peroxy radical with lower volatility. Autoxidation is eventually terminated by reaction with another radical such as hydroperoxyl ($HOO^•$) or a second peroxy radical from α-pinene. Examples of these final oxygenated monomers (C_{10} compounds) and covalently bound dimers (C_{20} compounds), respectively, from α-pinene are indicated by red squares. **b**, Aromatic organic vapours such as naphthalene (grey square) are oxidized in steps by hydroxyl radicals ($OH^•$)[66]. The first generation forms a peroxy radical ($(C_{10}H_8)(OH)OO^•$) and monomer products ($(C_{10}H_8)(OH)OOH$)). The monomer is more reactive with $OH^•$ and forms second-generation peroxy radicals ($(C_{10}H_8)(OH)_2(OOH)OO^•$) and monomers ($(C_{10}H_8)(OH)_2(OOH)_2$). Two peroxy radicals can combine to produce covalently bound dimers ($C_{20}H_{20}O_7$). ELVOC, extremely-low-volatility organic compounds; LVOC, low-volatility organic compounds; SVOC, semi-volatile organic compounds; IVOC, intermediate-volatility organic compounds; VOC, volatile organic compounds.

shown that the formation rates of H_2SO_4–NH_3 particles at 1.7 nm are enhanced by biogenic HOM[78,79], and reproduce observations in the boreal forest (Hyytiälä, Finland) both for nucleation and growth rates, and for molecular composition[44,50] (Fig. 3). However, it remains ambiguous whether this enhancement is truly a synergistic multi-component (H_2SO_4–NH_3–ULVOC) mechanism or co-condensation of two low-volatility chemical systems: (1) H_2SO_4–NH_3 and (2) ULVOC. The latter possibility is suggested by the absence of multi-component clusters in the mass spectra during nucleation events at either CLOUD or Hyytiälä (for example, Fig. 5 in ref. 44), although possible fragmentation of the clusters in the inlet of the mass spectrometer also needs to be considered[80].

In polluted urban environments, NPF rates span four orders of magnitude from 0.5 to 5,000 $cm^{-3}\,s^{-1}$ due to large variability in vapour concentrations and condensation sinks (Fig. 2). CLOUD experiments show that urban NPF is largely driven by sulfuric acid–base molecular clusters, stabilized by the presence of amines, high ammonia concentrations and low temperatures[67]. Although anthropogenic HOM play a minor role in nucleation, they drive particle growth, thereby affecting both the survival of newly formed particles and the mass concentration of smog episodes.

Sulfuric acid–ammonia–nitric acid

High concentrations of ammonium nitrate particles are observed in the upper troposphere over the Asian monsoon region[81] (Fig. 3). Ammonia dissolved in convected liquid cloud droplets is efficiently released upon freezing[82], after which it mixes with abundant nitric acid (HNO_3) from lightning. CLOUD experiments performed at upper tropospheric conditions show that H_2SO_4, NH_3 and HNO_3 form particles synergistically at rates that are orders-of-magnitude faster than those from any two of the three components[83]. Molar sulfate impurities as low as 1.7% can crystallize the ammonium nitrate to create highly efficient ice nuclei for cirrus clouds—comparable to desert dust[83].

At warm boundary layer temperatures, ammonia and nitric acid form semi-volatile particulate ammonium nitrate that then partitions between the gas and particle phases. CLOUD experiments have shown that non-equilibrium concentrations of ammonia and nitric acid in cities can drive ultra-rapid growth rates of few-nanometre-sized

particles that can reach 100–1,000 nm h^{-1} in short bursts that are hard to detect[84,85]. This may explain puzzling observations of NPF during smog episodes in Asian megacities despite high ambient condensation sinks above 0.01 s^{-1} that should rapidly quench NPF at apparent (averaged) growth rates[86].

Combining CLOUD results with models

The role of NPF in regulating global aerosol number concentrations and thereby influencing clouds and climate can only be quantified using atmospheric chemistry–aerosol–climate models. Experiments at CLOUD have identified the molecular mechanisms underlying NPF and, together with field studies, linked them to geographical locations (Fig. 3). In parallel, molecular models that describe the energetics and kinetics of particle nucleation and growth have been developed and tested against CLOUD data. Kinetic modelling, with evaporation rates determined from quantum chemical free energies (ΔG kcal mol^{-1}), has emerged as the most accurate method for describing atmospheric nucleation[87], and provides the basis for molecular models such as SAWNUC[88,89], ACDC[90] and MABNAG[91,92].

CLOUD measurements have provided an experimentally based understanding of the thermodynamics of H_2SO_4–NH_3 nucleation, upon which robust kinetic models have been built[12,93–95]. For more complex systems such as H_2SO_4–NH_3–ULVOC or HIO_3–HIO_2, simple empirical fits to NPF rates are available, for example, ref. 79, but parameterizations that embrace the more recent CLOUD findings are still under development. CLOUD is also measuring new gas-phase chemical reaction rates relevant for NPF[20,39,71]. In this way, CLOUD is providing mechanistic parameterizations of particle nucleation and growth for global models to address both climate[1,96] and the burden of disease[97]. Models based on CLOUD measurements show that ions account for 27% of global CCN at low cloud level (at 0.2% supersaturation)[1]. However, variations of galactic cosmic rays over the solar cycle lead to only 0.2% variation of CCN concentrations, which is not climatically significant[1].

Looking forwards

Advances in the understanding of NPF are needed to reduce the sources of urban smog, to sharpen estimates of Earth's climate sensitivity, and to anticipate how global and regional radiative forcings may change later this century as anthropogenic aerosols fall due to air quality policies. With CLOUD, we are presently studying NPF in cold regions of the atmosphere, simulating recent observations in the tropical upper free troposphere[56–58], Arctic[76] and Southern Ocean[98]. We have only recently been able to measure OH and HO_2 radicals in CLOUD, by laser-induced fluorescence[99]. Together with measurements of RO_2 and NO_x radicals, this will ensure realistic atmospheric conditions are simulated in the chamber for HOM experiments. These include the reaction rates for HOM formation over the full tropospheric temperature range, as well as studying the fate of the 90% fraction of organic vapours that undergo only one or two initial oxidation steps rather than autoxidation. We will also extend our studies of mixed chemical systems—acids, bases and HOM—and the role of ions in nucleation and cloud microphysics.

Experiments at CLOUD have measured NPF at the molecular level and helped to interpret observations in the ambient atmosphere. This mechanistic understanding has enabled the development of laboratory-based implementations of particle nucleation in global atmospheric chemistry and climate models. This is effectively catching up with gas-phase chemical kinetics where, for more than 40 years, laboratory experiments have provided straightforward kinetic equations that could be inserted directly into models—that is, explicit mechanisms. In the aerosol world, a similar level of 'nucleation kinetics' has largely been achieved through CLOUD experiments over the past 12 years. The inclusion of nucleation kinetics in climate models may substantially sharpen our understanding of aerosol radiative forcing.

Data availability

The CLOUD data are available from the published articles in the list of references and by request to their corresponding authors. Extended Data Table 2 provides the digital object identifier (doi) for selected CLOUD publications on nucleation and growth rates. The data for several CLOUD publications are already available on the Zenodo public repository (https://zenodo.org), hosted at CERN's Data Centre, and the data for the remaining publications will shortly be made available on Zenodo.

References

1. Gordon, H. et al. Causes and importance of new particle formation in the present-day and preindustrial atmospheres. *J. Geophys. Res. Atmos.* **122**, 8739–8760 (2017).
2. Kirkby, J. et al. Role of sulphuric acid, ammonia and galactic cosmic rays in atmospheric aerosol nucleation. *Nature* **476**, 429–433 (2011).
3. Kürten, A., Williamson, C., Almeida, J., Kirkby, J. & Curtius, J. On the derivation of particle nucleation rates from experimental formation rates. *Atmos. Chem. Phys.* **15**, 4063–4075 (2015).
4. Lee, S. et al. New particle formation in the atmosphere: from molecular clusters to global climate. *J. Geophys. Res. Atmos.* **124**, 7098–7146 (2019).
5. Kerminen, V.-M. et al. Atmospheric new particle formation and growth: review of field observations. *Environ. Res. Lett.* **13**, 103003 (2018).
6. Sellegri, K. et al. New particle formation: a review of ground-based observations at mountain research stations. *Atmosphere* **10**, 493 (2019).
7. Zhang, R. et al. Formation of urban fine particulate matter. *Chem. Rev.* **115**, 3803–3855 (2015).
8. O'Dowd, C. D. et al. Marine aerosol formation from biogenic iodine emissions. *Nature* **417**, 632–636 (2002).
9. Yu, F. & Turco, R. P. From molecular clusters to nanoparticles: role of ambient ionization in tropospheric aerosol formation. *J. Geophys. Res.* **106**, 4797–4814 (2001).
10. Schobesberger, S. et al. On the composition of ammonia–sulfuric-acid ion clusters during aerosol particle formation. *Atmos. Chem. Phys.* **15**, 55–78 (2015).
11. Olenius, T., Kupiainen-Määttä, O., Ortega, I. K., Kurtén, T. & Vehkamäki, H. Free energy barrier in the growth of sulfuric acid–ammonia and sulfuric acid–dimethylamine clusters. *J. Chem. Phys.* **139**, 084312 (2013).
12. Kürten, A. et al. Thermodynamics of the formation of sulfuric acid dimers in the binary (H_2SO_4–H_2O) and ternary (H_2SO_4–H_2O–NH_3) system. *Atmos. Chem. Phys.* **15**, 10701–10721 (2015).
13. Kürten, A. et al. Experimental particle formation rates spanning tropospheric sulfuric acid and ammonia abundances, ion production rates and temperatures. *J. Geophys. Res. Atmos.* **121**, 12377–12400 (2016).
14. Bianchi, F. et al. New particle formation in the free troposphere: a question of chemistry and timing. *Science* **352**, 1109–1112 (2016).
15. Bianchi, F. et al. The SALTENA experiment: comprehensive observations of aerosol sources, formation, and processes in the South American Andes. *Bull. Am. Met. Soc.* **103**, E212–E229 (2022).
16. Yan, C. et al. The role of H_2SO_4–NH_3 anion clusters in ion-induced aerosol nucleation mechanisms in the boreal forest. *Atmos. Chem. Phys.* **18**, 13231–13243 (2018).
17. Jokinen, T. et al. Ion-induced sulfuric acid–ammonia nucleation drives particle formation in coastal Antarctica. *Sci. Adv.* **4**, aat9744 (2018).
18. Lee, H. et al. Atmospheric new particle formation characteristics in the Arctic as measured at Mount Zeppelin, Svalbard, from 2016 to 2018. *Atmos. Chem. Phys.* **20**, 13425–13441 (2020).

19. Sarnela, N. et al. Measurement-model comparison of stabilized Criegee intermediate and highly oxygenated molecule production in the CLOUD chamber. *Atmos. Chem. Phys.* **18**, 2363–2380 (2018).
20. Shen, J. et al. High methanesulfonic acid production in the OH-initiated oxidation of dimethyl sulfide at low temperatures. *Environ. Sci. Technol.* https://doi.org/10.1021/acs.est.2c05154 (2022).
21. Chen, H. & Finlayson-Pitts, B. J. New particle formation from methanesulfonic acid and amines/ammonia as a function of temperature. *Environ. Sci. Technol.* **51**, 243–252 (2016).
22. Almeida, J. et al. Molecular understanding of sulphuric acid–amine particle nucleation in the atmosphere. *Nature* **502**, 359–363 (2013).
23. Kurtén, T., Loukonen, V., Vehkamäki, H. & Kulmala, M. Amines are likely to enhance neutral and ion-induced sulfuric acid–water nucleation in the atmosphere more effectively than ammonia. *Atmos. Chem. Phys.* **8**, 4095–4103 (2008).
24. Kürten, A. et al. Neutral molecular cluster formation of sulfuric acid–dimethylamine observed in real time under atmospheric conditions. *Proc. Natl Acad. Sci. USA* **111**, 15019–15024 (2014).
25. Cai, R. et al. The missing base molecules in atmospheric acid–base nucleation. *Natl. Sci. Rev.* **9**, nwac137 (2022).
26. Bianchi, F. et al. Insight into acid–base nucleation experiments by comparison of the chemical composition of positive, negative, and neutral clusters. *Environ. Sci. Technol.* **48**, 13675–13684 (2014).
27. Kürten, A. et al. New particle formation in the sulfuric acid–dimethylamine–water system: reevaluation of CLOUD chamber measurements and comparison to an aerosol nucleation and growth model. *Atmos. Chem. Phys.* **18**, 845–863 (2018).
28. Stolzenburg, D. et al. Enhanced growth rate of atmospheric particles from sulfuric acid. *Atmos. Chem. Phys.* **20**, 7359–7372 (2020).
29. Lehtipalo, K. et al. The effect of acid–base clustering and ions on the growth of atmospheric nano-particles. *Nature Commun.* **7**, 11594 (2016).
30. Rondo, L. et al. Effect of dimethylamine on the gas phase sulfuric acid concentration measured by Chemical Ionization Mass Spectrometry (CIMS). *J. Geophys. Res. Atmos.* **121**, 3036–3049 (2016).
31. Ge, X., Wexler, A. S. & Clegg, S. L. Atmospheric amines - Part I. A review. *Atmos. Environ.* **45**, 524–546 (2011).
32. Hanson, D. R., McMurry, P. H., Jiang, J., Tanner, D. & Huey, L. G. Ambient pressure proton transfer mass spectrometry: detection of amines and ammonia. *Environ. Sci. Technol.* **45**, 8881–8888 (2011).
33. Yao, L. et al. Atmospheric new particle formation from sulfuric acid and amines in a Chinese megacity. *Science* **361**, 278–281 (2018).
34. Yin, R. et al. Acid–base clusters during atmospheric new particle formation in urban Beijing. *Environ. Sci. Technol.* **55**, 10994–11005 (2021).
35. Smith, J. N. et al. Observations of aminium salts in atmospheric nanoparticles and possible climatic implications. *Proc. Natl Acad. Sci. USA* **107**, 6634–6639 (2010).
36. Creamean, J. M. et al. Measurements of aerosol chemistry during new particle formation events at a remote rural mountain site. *Environ. Sci. Technol.* **45**, 8208–8216 (2011).
37. Brean, J. et al. Open ocean and coastal new particle formation from sulfuric acid and amines around the Antarctic Peninsula. *Nat. Geosci.* **14**, 383–388 (2021).
38. Sindelarova, K. et al. Global data set of biogenic VOC emissions calculated by the MEGAN model over the last 30 years. *Atmos. Chem. Phys.* **14**, 9317–9341 (2014).
39. Molteni, U. et al. Formation of highly oxygenated organic molecules from α-pinene ozonolysis: chemical characteristics, mechanism, and kinetic model. *ACS Earth Space Chem.* **3**, 873–883 (2019).
40. Bianchi, F. et al. Highly oxygenated organic molecules (HOM) from gas-phase autoxidation involving peroxy radicals: a key contributor to atmospheric aerosol. *Chem. Rev.* **119**, 3472–3509 (2019).
41. Kirkby, J. et al. Ion-induced nucleation of pure biogenic particles. *Nature* **533**, 521–526 (2016).
42. Zhang, R. et al. Atmospheric new particle formation enhanced by organic acids. *Science* **304**, 1487–1490 (2004).
43. Elm, J., Myllys, N. & Kurtén, T. What is required for highly oxidized molecules to form clusters with sulfuric acid? *J. Phys. Chem. A* **121**, 4578–4587 (2017).
44. Lehtipalo, K. et al. Multi-component new particle formation from sulfuric acid, ammonia, and biogenic vapors. *Sci. Adv.* **4**, 12 (2018).
45. Frege, C. et al. Influence of temperature on the molecular composition of ions and charged clusters during pure biogenic nucleation. *Atmos. Chem. Phys.* **18**, 65–79 (2018).
46. Simon, M. et al. Molecular understanding of new particle formation from α-pinene between −50 °C and 25 °C. *Atmos. Chem. Phys.* **20**, 9183–9207 (2020).
47. Ye, Q. et al. Molecular composition and volatility of nucleated particles from α-pinene oxidation between −50 °C and +25 °C. *Environ. Sci. Technol.* **53**, 12537–12365 (2019).
48. Tröstl, J. et al. The role of low-volatility organic compounds to initial particle growth in the atmosphere. *Nature* **533**, 527–531 (2016).
49. Stolzenburg, D. et al. Rapid growth of organic aerosol nanoparticles over a wide tropospheric temperature range. *Proc. Natl Acad. Sci. USA* **115**, 9122–9127 (2018).
50. Kulmala, M. et al. Direct observations of atmospheric aerosol nucleation. *Science* **339**, 943–946 (2013).
51. McFiggans, G. et al. Secondary organic aerosol reduced by mixture of atmospheric vapours. *Nature* **565**, 587–593 (2019).
52. Heinritzi, M. et al. Molecular understanding of the suppression of new particle formation by isoprene. *Atmos. Chem. Phys.* **20**, 11809–11821 (2020).
53. Yan, C. et al. Size-dependent influence of NO_x on the growth rates of organic aerosol particles. *Sci. Adv.* **6**, eaay4945 (2020).
54. Nie, W. et al. NO at low concentration can enhance the formation of highly oxygenated biogenic molecules in the atmosphere. *Nat. Commun.* **14**, 3347 (2023).
55. Dada, L. et al. Role of sesquiterpenes in biogenic new particle formation. *Sci. Adv.* **9**, eadi5297 (2023).
56. Andreae, M. O. et al. Aerosol characteristics and particle production in the upper troposphere over the Amazon Basin. *Atmos. Chem. Phys.* **18**, 921–961 (2018).
57. Williamson, C. J. et al. A large source of cloud condensation nuclei from new particle formation in the tropics. *Nature* **574**, 399–403 (2019).
58. Zha, Q. et al. Oxidized organic molecules in the tropical free troposphere over Amazonia. *Natl Sci. Rev.* https://doi.org/10.1093/nsr/nwad138 (2023).
59. Wang, X., Gordon, H., Grosvenor, D. P., Andreae, M. O. & Carslaw, K. S. Contribution of regional aerosol nucleation to low-level CCN in an Amazonian deep convective environment: results from a regionally nested global model. *Atmos. Chem. Phys.* **23**, 4431–4461 (2023).
60. Carslaw, K. S. et al. Large contribution of natural aerosols to uncertainty in indirect forcing. *Nature* **503**, 67–71 (2013).
61. Gordon, H. et al. Reduced anthropogenic aerosol radiative forcing caused by biogenic new particle formation. *Proc. Natl Acad. Sci. USA* **113**, 12053–12058 (2016).

62. Rose, C. et al. Observations of biogenic ion-induced cluster formation in the atmosphere. *Sci. Adv.* **4**, eaar5218 (2018).
63. Bianchi, F. et al. Biogenic particles formed in the Himalaya as an important source of free tropospheric aerosols. *Nat. Geosci.* **14**, 4–9 (2020).
64. Andreae, M. O., Andreae, T. W., Ditas, F. & Pöhlker, C. Frequent new particle formation at remote sites in the subboreal forest of North America. *Atmos. Chem. Phys.* **22**, 2487–2505 (2022).
65. Suni, T. et al. Formation and characteristics of ions and charged aerosol particles in a native Australian eucalypt forest. *Atmos. Chem. Phys.* **8**, 129–139 (2008).
66. Wang, M. et al. Photo-oxidation of aromatic hydrocarbons produces low-volatility organic compounds. *Environ. Sci. Technol.* **54**, 7911–7921 (2020).
67. Xiao, M. et al. The driving factors of new particle formation and growth in the polluted boundary layer. *Atmos. Chem. Phys.* **21**, 14275–14291 (2021).
68. Sipilä, M. et al. Molecular-scale evidence of aerosol particle formation via sequential addition of HIO_3. *Nature* **537**, 532–534 (2016).
69. He, X.-C. et al. Role of iodine oxoacids in atmospheric aerosol nucleation. *Science* **371**, 589–595 (2021).
70. Zhang, R. et al. Critical role of iodous acid in neutral iodine oxoacid nucleation. *Environ. Sci. Technol.* **56**, 14166–14177 (2022).
71. Finkenzeller, H. et al. The gas-phase formation mechanism of iodic acid as an atmospheric aerosol source. *Nat. Chem.* **15**, 129–135 (2023).
72. Cuevas, C. A. et al. Rapid increase in atmospheric iodine levels in the North Atlantic since the mid-20th century. *Nat. Commun.* **9**, 1452–1457 (2018).
73. Grose, M. R., Cainey, J. M., McMinn, A. & Gibson, J. A. E. Coastal marine methyl iodide source and links to new particle formation at Cape Grim during February 2006. *Environ. Chem.* **4**, 172–177 (2007).
74. Mahajan, A. S. et al. Concurrent observations of atomic iodine, molecular iodine and ultrafine particles in a coastal environment. *Atmos. Chem. Phys.* **11**, 2545–2555 (2011).
75. Yu, H. et al. Iodine speciation and size distribution in ambient aerosols at a coastal new particle formation hotspot in China. *Atmos. Chem. Phys.* **19**, 4025–4039 (2019).
76. Baccarini, A. et al. Frequent new particle formation over the high Arctic pack ice by enhanced iodine emissions. *Nat. Commun.* **11**, 4924 (2020).
77. Glasoe, W. A. et al. Sulfuric acid nucleation: an experimental study of the effect of seven bases. *J. Geophys. Res. Atmos.* **120**, 1933–1950 (2015).
78. Schobesberger, S. et al. Molecular understanding of atmospheric particle formation from sulfuric acid and large oxidized organic molecules. *Proc. Natl Acad. Sci. USA* **110**, 17223–17228 (2013).
79. Riccobono, F. et al. Oxidation products of biogenic emissions contribute to nucleation of atmospheric particles. *Science* **344**, 717–721 (2014).
80. Zapadinsky, E., Passananti, M., Myllys, N., Kurtén, T. & Vehkamäki, H. Modeling on fragmentation of clusters inside a mass spectrometer. *J. Phys. Chem. A* **123**, 611–624 (2019).
81. Höpfner, M. et al. Ammonium nitrate particles formed in upper troposphere from ground ammonia sources during Asian monsoons. *Nat. Geosci.* **12**, 608–612 (2019).
82. Ge, C., Zhu, C., Francisco, J. S., Zeng, X. C. & Wang, J. A molecular perspective for global modeling of upper atmospheric NH_3 from freezing clouds. *Proc. Natl Acad. Sci. USA* **115**, 6147–6152 (2018).
83. Wang, M. et al. Synergistic HNO_3–H_2SO_4–NH_3 upper tropospheric particle formation. *Nature* **605**, 483–489 (2022).
84. Wang, M. & Kong, W. et al. Rapid growth of new atmospheric particles by nitric acid and ammonia condensation. *Nature* **581**, 184–189 (2020).
85. Marten, R. et al. Survival of newly formed particles in haze conditions. *Environ. Sci. Atmos.* **2**, 491–499 (2022).
86. Kulmala, M. et al. Atmospheric gas-to-particle conversion: why NPF events are observed in megacities? *Faraday Disc.* **200**, 271–288 (2017).
87. Olenius, T., Yli-Juuti, T., Elm, J., Kontkanen, J. & Riipinen, I. in *Physical Chemistry of Gas–Liquid Interfaces* (eds. Faust, J. A. & House, J. E.) 315–352 (Elsevier, 2018).
88. Lovejoy, E. R., Curtius, J. & Froyd, K. D. Atmospheric ion-induced nucleation of sulfuric acid and water. *J. Geophys. Res. Atmos.* https://doi.org/10.1029/2003JD004460 (2004).
89. Ehrhart, S. et al. Comparison of the SAWNUC model with CLOUD measurements of sulphuric acid–water nucleation. *J. Geophys. Res. Atmos.* **121**, 12401–12414 (2016).
90. McGrath, M. J. et al. Atmospheric Cluster Dynamics Code: a flexible method for solution of the birth–death equations. *Atmos. Chem. Phys.* **12**, 2345–2355 (2012).
91. Yli-Juuti, T. et al. Model for acid–base chemistry in nanoparticle growth (MABNAG). *Atmos. Chem. Phys.* **13**, 12507–12524 (2013).
92. Ahlm, L. et al. Modeling the thermodynamics and kinetics of sulfuric acid–dimethylamine–water nanoparticle growth in the CLOUD chamber. *Aerosol Sci. Technol.* **50**, 1017–1032 (2016).
93. Määttänen, A. et al. New parameterizations for neutral and ion-induced sulfuric acid-water particle formation in nucleation and kinetic regimes. *J. Geophys. Res. Atmos.* **123**, 1269–1296 (2018).
94. Yu, F. et al. H_2SO_4–H_2O–NH_3 ternary ion-mediated nucleation (TIMN): kinetic-based model and comparison with CLOUD measurements. *Atmos. Chem. Phys.* **18**, 17451–17474 (2018).
95. Kürten, A. New particle formation from sulfuric acid and ammonia: nucleation and growth model based on thermodynamics derived from CLOUD measurements for a wide range of conditions. *Atmos. Chem. Phys.* **19**, 5033–5050 (2019).
96. Dunne, E. et al. Global atmospheric particle formation from CERN CLOUD measurements. *Science* **354**, 1119–1124 (2016).
97. Lelieveld, J. et al. Effects of fossil fuel and total anthropogenic emission removal on public health and climate. *Proc. Natl Acad. Sci. USA* **116**, 7192–7197 (2019).
98. McCoy, I. L. et al. Influences of recent particle formation on Southern Ocean aerosol variability and low cloud properties. *J. Geophys. Res. Atmos.* **126**, e2020JD033529 (2021).
99. Novelli, A. et al. Characterisation of an inlet pre-injector laser-induced fluorescence instrument for the measurement of atmospheric hydroxyl radicals. *Atmos. Meas. Tech.* **7**, 3413–3430 (2014).
100. Schervish, M. & Donahue, N. M. Peroxy radical chemistry and the volatility basis set. *Atmos. Chem. Phys.* **20**, 1183–1199 (2020).

Acknowledgements

We thank the many scientists who performed the CLOUD research reported here. We thank the European Organization for Nuclear Research (CERN) for supporting CLOUD with important technical and financial resources and for providing a particle beam from the CERN Proton Synchrotron. We thank our research institutes, national funding agencies and the European Union for providing financial support for the CLOUD experiment. We gratefully acknowledge financial support from the following sources: the German Ministry of Science and Education (CLOUD-22, 01LK2201), ACCC Flagship programme of the Academy of Finland (grant nos. 337549 and 337550), the Academy of Finland (grant no. 336557), the Swiss National Science Foundation (SNF grant no. 200021_213071), the Faculty of Physics at the University of Vienna, the University of Tartu (grant no. PRG714), Horizon 2020 (EMME-CARE, 857712), Horizon Europe MSCA-DN (CLOUD-DOC, 101073026), the NASA ROSES programme (grant no. 80NSSC19K0949) and the United States National Science Foundation (NSF grant nos. NSF-AGS-2215527, NSF-AGS-1602086,

NSF-AGS-213208, NSF-AGS-2215489, NSF-AGS-2027252 and NSF-AGS-2215522).

Author contributions

J.K., A.A., U.B., K.S.C, T.C., J.C, N.M.D., I.E.H., R.C.F., H.G., A.H., H.H., H.J., M.K., A.K., A.L., K.L., J.L., O.M., I.R., F.S., A.T., A.V., R.V., P.M.W. and D.R.W. contributed to the CLOUD research reported in the manuscript. J.K. wrote the manuscript. J.K. prepared Figs. 1–3, and N.M.D. prepared Fig. 4 together with J.K. All authors contributed to and approved the final version of the manuscript.

Competing interests

The authors declare no competing interests.

Additional information

Extended data is available for this paper at https://doi.org/10.1038/s41561-023-01305-0.

Correspondence should be addressed to Jasper Kirkby.

Peer review information *Nature Geoscience* thanks Song Guo, Fangqun Yu and the other, anonymous, reviewer(s) for their contribution to the peer review of this work. Primary Handling Editor: Xujia Jiang, in collaboration with the *Nature Geoscience* team.

https://doi.org/10.1038/s41561-023-01305-0

Extended Data Table 1 | Range of parameters for all CLOUD experiments

Parameter	Units	Lower	Upper	Comments
Chamber conditions:				
Temperature	K	208	308	Chamber cleaning at 373 K
Relative pressure	mbar	5	220	Relative to atmospheric pressure
Relative humidity (RH)	%	0	140	Adiabatic pressure reductions for RH > 100%
Mixing fans speed	%	12	100	Standard operation is 12%
Wall loss rate	s^{-1}	2.2E-3	1.0E-2	For 12%→100% fans speed, respectively
Dilution rate	s^{-1}	1E-4	2.4E-4	Chamber volume is 26.1 m^{-3}
Contaminants:				
Sulfuric acid (H_2SO_4)	cm^{-3}	-	<2E4	Below the limit of detection (LoD)
Ammonia (NH_3)	pptv	0.01	<4	Between 208K→278K (80% RH), respectively
Dimethylamine (C_2H_7N)	pptv	-	<0.01	Below the LoD
Light organics (C_{1-3})	pptv	-	<150	
Heavy organics (≥C_5)	pptv	-	<1	Below the LoD
Iodic acid (HIO_3)	pptv	-	<0.01	Below the LoD
Optical power:				
Hg-Xe lamps	W	0.15	15	230–700 nm fibre optic
KrF excimer laser	W	0.01	10	248 nm fibre optic
Light sabre 1	W	52	52	254 nm low pressure Hg lamp
Light sabre 3	W	20	447	385 nm LED array
Light sabre 4	W	6	153	528 nm LED array
Ionisation rate:				
Galactic cosmic rays	ip$cm^{-3}s^{-1}$	0	2	20 kV/m electric field for zero ions
Beam muon background	ip$cm^{-3}s^{-1}$	0	6	When CERN Proton Synchrotron is in operation
Pion beam	ip$cm^{-3}s^{-1}$	10	100	Collimator adjustment
Trace vapours:				
Ozone (O_3)	ppbv	0	300	Chamber cleaning at 3 ppm
Sulfur dioxide (SO_2)	ppbv	0	10	
Dimethyl sulfide (C_2H_6S)	ppbv	0	4	
Sulfuric acid (H_2SO_4)	cm^{-3}	<2E4	1E9	
Methanesulfonic acid (CH_3SO_3H)	cm^{-3}	0	1E8	
Nitric acid (HNO_3)	pptv	0	1000	
Nitrous acid (HONO)	pptv	0	1000	
Nitrogen oxides (NO_x)	pptv	0	5000	
Ammonia (NH_3)	pptv	<4	3000	
Dimethylamine (C_2H_7N)	pptv	<0.01	140	
Hydrogen (H_2)	%	0	0.1	
Carbon monoxide (CO)	ppmv	0.1	50	
Methane (CH_4)	ppbv	<1	2600	
Glyoxal ($C_2H_2O_2$)	ppbv	0	4	
Isoprene (C_5H_8)	pptv	0	1E4	
α-pinene ($C_{10}H_{16}$)	pptv	0	2500	
Δ-3-carene ($C_{10}H_{16}$)	pptv	0	1200	
Limonene ($C_{10}H_{16}$)	pptv	0	1200	
Pinanediol ($C_{10}H_{18}O_2$)	pptv	0	2E4	
β-caryophyllene ($C_{15}H_{24}$)	pptv	0	16	
Toluene (C_7H_8)	ppbv	0	50	
Trimethylbenzene (C_9H_{12})	ppbv	0	10	
Naphthalene ($C_{10}H_8$)	ppbv	0	5	
Cresol (C_7H_8O)	ppbv	0	2	
Iodine (I_2)	pptv	0	100	
Diiodomethane (CH_2I_2)	pptv	0	100	

A vapour mixing ratio of 1 pptv (part per trillion by volume) is equivalent to a concentration of 2.5×10^7 molecules cm^{-3}. The notation 2.2E-3 represents 2.2×10^{-3}.

https://doi.org/10.1038/s41561-023-01305-0

Extended Data Table 2 | Range of parameters for selected CLOUD nucleation and growth rate experiments

Chemical system/Reference & doi	T[K]	RH[%]	O_3[ppbv]	H_2SO_4[cm^{-3}]	NH_3[pptv]	DMA[pptv]	$C_{10}H_{16}$[pptv]	Other[pptv]
H_2SO_4 - NH_3:								
Kirkby et al. 2011[2]	248-292	38	50-300	5E6-1E8	10-1500	0	0	0
https://doi.org/10.1038/nature10343								
Dunne et al. 2016[96]	208-298	20-74	40	5E5-1E9	0.01-1400	0	0	0
https://doi.org/10.1126/science.aaf2649								
Kürten et al. 2016[13]	208-298	20-74	40	5E5-1E9	0.01-1400	0	0	0
https://doi.org/10.1002/2015JD023908								
Stolzenburg et al. 2020[28]	278-293	38-60	120	2E7-1E9	3-1000	0	0	0
https://doi.org/10.5194/acp-20-7359-2020								
H_2SO_4 - DMA:								
Almeida et al. 2013[22]	278	38	40	5E5-3E8	4-250	0-140	0	0
https://doi.org/10.1038/nature12663								
Kürten et al. 2018[27]	278	38	40	1E6-3E7	<4	40	0	0
https://doi.org/10.5194/acp-18-845-2018								
Biogenic HOM:								
Kirkby et al. 2016[41]	278	5-80	25-35	<2E4-6E6	<4	0	0-1300	0
https://doi.org/10.1038/nature17953								
Stolzenburg et al. 2018[49]	248-298	38	30-40	<2E4	<4	0	200-1400	0
https://doi.org/10.1073/pnas.1807604115								
Simon et al. 2020[46]	223-298	40-90	37-48	<2E4	<4	0	200-2000	0
https://doi.org/10.5194/acp-20-9183-2020								
Heinritzi et al. 2020[52]	278-298	38	35-40	<2E4	<4	0	330-2500	
https://doi.org/10.5194/acp-20-11809-2020								
C_5H_8								0-1E4
Dada et al. 2023[55]	278-298	5-90	40	<2E4	<4	0	200-1200	
https://doi.org/10.1126/sciadv.adi5297								
C_5H_8								0-1E4
$C_{15}H_{24}$								0-16
NO_x								0-300
HIO_3 - HIO_2:								
He et al. 2021[69]	263-273	34-73	40	<2E4	<4	0	0	
https://doi.org/10.1126/science.abe0298								
HIO_3								1E6-2E8
H_2SO_4 - NH_3 - biogenic HOM:								
Lehtipalo et al. 2018[44]	278	38	40	1E6-7E7	4-3000	0	100-1500	
https://doi.org/10.1126/sciadv.aau5363								
NO_x								0-5E3
H_2SO_4 - NH_3 - DMA - anthropogenic HOM:								
Xiao et al. 2021[67]	278-293	57	40	6E5-8E7	70-2000	0-4	0	
https://doi.org/10.5194/acp-21-14275-2021								
C_7H_8								0-5E4
C_9H_{12}								0-1E4
$C_{10}H_8$								0-5E3
NO_x								0-1.5E3
H_2SO_4 - NH_3 - HNO_3:								
Wang, Kong et al. 2020[84]	248-293	25	40	1E7-6E7	22-2500	0	0	
https://doi.org/10.1038/s41586-020-2270-4								
HNO_3								0-1000
NO_2								0-1E4
Wang et al. 2022[83]	223	25	40	0-2E6	0.1-25	0	0	
https://doi.org/10.1038/s41586-022-04605-4								
HNO_3								0-50

The trace vapour corresponding to a value shown in the final column (labelled "Other") is indicated at the start of that row. The chemical compounds corresponding to formulae shown in the table can be found in Table S1. RH indicates relative humidity and DMA indicates dimethylamine (C_2H_7N). The notation 5E6 represents 5×10^6.